A critical review of the sedimentary record of the 'Millennium Eruption' of Changbaishan/Paektu-san volcano

Qingyuan Yang[*, 1,2], Susanna F Jenkins[1,2], Geoffrey A Lerner[1,2,3], Clive Oppenheimer[4], Amy Donovan[4], James O. S. Hammond[5], Haiquan Wei[6], Jiandong Xu[6], Bo Pan[6] and Ryo Nakanishi[7,8]

[*]qingyuan.yang@ntu.edu.sg

[1]Earth Observatory of Singapore, Singapore, 639798, Singapore

[2]Asian School of the Environment, Nanyang Technological University, Singapore, 639798, Singapore

[3]Now at Instituto de Geofísica, National Autonomous University of Mexico, Mexico City, 04510, Mexico

[4]Department of Geography, University of Cambridge, Downing Place, Cambridge, CB2 3EN, UK

[5]Department of Earth and Planetary Sciences, Birkbeck College, University of London, London, WC1E 7HX, UK

[6]National Observation and Research Station of Jilin Changbaishan Volcano, Institute of Geology, China Earthquake Administration, Beijing, 100029, China

[7]Atmosphere and Ocean Research Institute, The University of Tokyo, Kashiwa 277-8564, Japan

[8]Graduate School of Frontier Sciences, The University of Tokyo, Kashiwa, 277-8561, Japan

September 28, 2022

Abstract

The 'Millennium Eruption' of Changbaishan/Paektu-san Volcano, situated today on border between the People's Republic of China and Democratic People's Republic of Korea, ranks as one of the largest eruptions of the Common Era. Dated to 946 CE, its tephra deposits represent a critical marker spanning terrestrial and marine archives, as well as the glacial record of Greenland. Its geographically extensive footprint, along with the great magnitude of the eruption, have drawn wide attention from scholars working in different disciplines and representing different national and international groups. While much has been achieved through programmes of field and laboratory research, particularly sedimentological, tephrostratigraphic and petrographic studies, a universally accepted stratigraphy and timeline for the eruption episode have yet to be realised. The lack of consensus and discrepancies in interpretations of the deposits reflect, in part, the paucity and ambiguity in interpreting outcrops and historical records of the eruption, as well, arguably, as the geopolitical challenges of conducting international fieldwork

in a sensitive border region. Here, we interrogate the scientific literature on the Millennium Eruption with the aims of highlighting points of contention, reconciling disparate observations where possible, and proposing new interpretations of existing data. We hope thereby to provide a clear foundation for future studies to use to build towards a coherent stratigraphic and sedimentological interpretation of the proximal tephra record, and new understanding of the compositional, stratigraphic and spatial variations of the distal deposits. Such a research agenda will lead to an improved reconstruction of this iconic volcanic eruption, which will offer wider implications for understanding the contemporary regional history and archaeology, as well as the potential environmental, ecological and climatological impacts of the eruption.

1 Introduction

Changbaishan/Paektu-san Volcano is a Cenozoic polygenetic central volcano (Haiquan et al., 1999; Wei et al., 2003) located on the border of People's Republic of China (China) and Democratic People's Republic of Korea (DPRK; Fig. 1). Its eruptive history from late Pleistocene to Holocene and recent unrest from 2002 to 2005 indicate that the volcano presents a number of hazards for local communities, infrastructure, and aviation safety (e.g., Wei et al., 2013; Yu et al., 2013). Tephra fall deposits from previous eruptions of Changbaishan/Paektu-san Volcano were widely dispersed, making them valuable regional to global tephra isochrons (e.g., Nanayama et al., 2003; Xu et al., 2013; Sun et al., 2014a; McLean et al., 2016; Chen et al., 2016; McLean et al., 2020).

The most recent voluminous eruption of the Changbaishan/Paektu-san Volcano took place in late 946 CE (Xu et al., 2013; Oppenheimer et al., 2017), and is named the "Millennium Eruption" (ME). The Volcanic Explosivity Index (VEI) of the ME was recently revised from 7 to 6 (Yang et al., 2021). The eruptive products of the ME have been studied using various methods in previous works (e.g., Wei et al., 2007; Zou et al., 2010; Yin et al., 2012; Cheong et al., 2019; Ramos et al., 2019; Kuritani et al., 2020). Thanks to these works, our understanding of the ME has improved. All studies agree that the ME was a major explosive event with two distinct phases, both generating tephra fallout and pyroclastic density currents. However, a range of new observations, data, and interpretations on the ME and its eruptive products (e.g., Shi et al., 2005; Sun et al., 2017; Pan et al., 2017; Ramos et al., 2019; Pan et al., 2020), have reached conclusions that are not readily reconciled with each other. For example, whether comenditic material was produced during Phase 2 of the ME is a matter of dispute (Machida et al., 1990; Pan et al., 2017; Sun et al., 2017; Pan et al., 2020), and a universal stratigraphy for the deposits is lacking. Such information is fundamental and critical to our understanding of the ME.

In addition to producing new data and interpretations, it is necessary to integrate and re-evaluate previous works in the light of new studies. Detailed and careful reviews have been carried out on the ME and the Changbaishan/Paektu-san Volcano from different perspectives (Wei et al., 2013; Sun et al., 2014b; Zhang et al., 2018; Wei et al., 2021), but a review focusing on (1) physical and stratigraphical characteristics of the ME eruptive products and their spatial correlation and (2) eruptive processes during the ME has not been undertaken. In addition, to address differences of opinion concerning the ME, it is important to study not only the points of contention themselves but also the corresponding supporting observations and data. Only in this way can we find out why such disputes have not been resolved and what data are needed to address them.

Our aims here are to (1) review previous works on pyroclastic fall and density current deposits of the ME and potentially post-ME eruptions with a focus on their stratigraphic features and spatial unit correlation;

(2) highlight areas of contention and resolve their origins; (3) and propose new interpretations, questions, and hypotheses to guide future studies of the ME and any subsequent deposits. We evaluate whether apparently conflicting interpretations in previous works are necessarily mutually exclusive.

In the following text, we give a brief overview of the ME. We review its eruptive products from old to new and from proximal to distal. For each eruptive product, we first list its characteristics and interpretations that are not in dispute, and then discuss the disputes, propose our own interpretations, or point out what might be important for future studies. We then discuss critical and open questions associated with the ME.

Disputes on eruptive products of the ME are convoluted and at different levels, from field observations to experimental data to geological interpretations. One dispute could interact and affect the others. These disputes are complex, and so we attempt to address them in detail, before summarizing them in a way that is as clear as possible without oversimplification.

2 Overview of the ME

The ME began in late 946, CE (Xu et al., 2013; Oppenheimer et al., 2017). Based on historical records (Hayakawa and Koyama, 1998) and tephra stratigraphy in Japan (McLean et al., 2016), Oppenheimer et al. (2017) have suggested a date of 2, November. The ME has two phases which were dominated by comenditic and trachytic eruptive materials respectively. Phase 1 of the ME began with a plinian eruption that produced widely dispersed tephra (Machida et al., 1990; Horn and Schmincke, 2000) followed by pyroclastic flows and surges (Machida et al., 1990). Phase 2 of the ME produced agglutinates, multiple tephra layers, and pyroclastic flow and surge deposits (Machida et al., 1990; Horn and Schmincke, 2000; Pan et al., 2017). Some have suggested that there was a short hiatus between the two phases (Machida et al., 1990; Pan et al., 2020; Sun et al., 2017).

It is estimated that the ME produced $40-98$ km^3 (bulk volume; Yang et al., 2021) of pyroclastic material in total with a maximum column height of 25-35 km during Phase 1 (Liu et al., 1998; Wei et al., 2003; Yu et al., 2013). Liu et al. (1998) estimated the total eruption duration (excluding the hiatus between the two phases) to be between five days and two weeks.

Volcanic ash produced from the ME was dispersed as far as Japan and even Greenland, where a few grains of both comenditic and trachytic composition have been identified (Sun et al., 2014a). Distal ash from the ME is also known as the Baegdusan—Tomakomai (B-Tm) ash (Machida and Arai, 1983), and is used as a regional tephra marker in many studies (e.g., Chen et al., 2016; McLean et al., 2016, 2020). Whether or not there were eruptions after the ME remains a point of dispute (e.g., Ramos et al., 2016; Sun et al., 2017; Ramos et al., 2019; Pan et al., 2020)

3 Proximal Phase 1 tephra

The Phase 1 tephra deposit is represented in a widely dispersed white, comenditic pumice fallout. It is widespread close to the volcano (Fig. 1) and composed of highly vesicular light-colored pumice. It is well-sorted and exhibits complex grading at some localities (Machida et al., 1990). Lithics include older basalt and trachyte of the stratocone, and syenite, traychyandesitic volcanic and granite clasts (Horn and Schmincke, 2000; Sun et al., 2017). Minor amounts of mixed or banded pumice and trachyandesitic scorias are also present (Machida et al., 1990; Horn and Schmincke, 2000; Sun et al., 2017; Pan et al., 2017). Physical characteristics of the Phase 1 tephra are summarized in Table 1. The Phase 1 tephra were dispersed to the

east and southeast with its isopachs given in Horn and Schmincke (2000). Its northern extent was delineated by Machida et al. (1990), and presented here in Fig. 6c.

The Phase 1 tephra has well-constrained high silica content (Fig. 3). The banded pumice, characterized by a wide and continuous range of SiO_2 concentration (Fig. 2a; Sun et al., 2017; Pan et al., 2017), was also produced during Phase 1, indicative of magma mixing during the ME (Pan et al., 2017).

3.1 Uncertainty on the origin of the newly discovered comenditic ash to the northeast of the caldera

Comenditic tephra have been recently found in peatland cores YLW and DFH 29 km northeast of the caldera (Fig. 1; Zhang et al., 2022a,b). At these sites, the comenditic ash underlies trachytic tephra, and was hence attributed to Phase 1 (Zhang et al., 2022a,b). We include these observations in the isopach map in Fig. 6a, revealing a lobe of fallout to the northeast of the caldera, that is not consistent with the overall Phase 1 tephra dispersal pattern (Fig. 6)

The grain size of the comenditic tephra at sites YLW and DFW is also much finer than the overlying trachytic tephra (Fig. 2 in Zhang et al., 2022b), which is very uncommon if the lower comenditic tephra was from a plinian column during Phase 1 (Machida et al., 1990). As Phase 2 of the ME might also produce comenditic tephra (explained in more detail later; Machida et al., 1990; Sun et al., 2017), based on current evidence, we cannot exclude the possibility that the comendite at sites YLW and DFH was, in fact, from Phase 2 of the ME.

4 Proximal Phase 1 pyroclastic flow of the ME

The Phase 1 pyroclastic flow deposit was emplaced after the Phase 1 tephra. The flow and tephra deposits do not interbed each other. Co-ignimbrite ash fallout occurred (Pan et al., 2017). The pyroclastic flow deposit has an estimated average thickness of ∼5 m and is found on all gentle slopes of the volcano and lower flood plains mainly to the northeast and west of the caldera in the Chinese territory (Machida et al., 1990; Zhao et al., 2020). The extent of pyroclastic flow deposits from the ME (i.e., union of flow deposit extents from the two phases) in the Chinese territory was mapped by Zhao et al. (2020). This extent also characterizes the Phase 1 flow extent in the Chinese territory (as the Phase 1 flow extent is greater and covers the Phase 2 flow). We are unaware of any detailed published studies of the Phase 1 flow deposit in DPRK.

Machida et al. (1990), Shi et al. (2005), and Sun et al. (2017) observed that the Phase 1 flow deposit was non-welded, and composed of light- and dark-colored pumice, glass shards, lithic fragments with abundant carbonized tree stems, and banded pumice clasts are common. The Phase 1 pyroclastic flow can be easily recognized in the field owing to its distinct light grey colour and the presence of carbonized woods (Table 1).

4.1 On the presence of trachyte in the Phase 1 flow

Whether the sampled pumice from the ME flow deposits were from Phase 1 and/or 2 is not always specified in previous studies, making it difficult to compare them. It is known that the Phase 1 flow pumice is dominantly comenditic and has banded pumice, but Machida et al. (1990) also found compositional bimodality (i.e., comendite and trachyte) in their Phase 1 flow pumice samples from two locations (Fig. 2d and Fig. 3), suggesting the potential presence of trachytic material within the Phase 1 flow. We found neither corroborating or negating evidence for this observation.

Pumice samples from the ME pyroclastic flow at site XGFSL ∼ 18 km northeast of the caldera are characterized by a wide range of silica content (Fig. 2b; Sun et al., 2017), similar to those reported in Machida et al. (1990), but stratigraphic positions of the samples are not specified. This makes it difficult to tell whether the samples were from Phase 1 or (and) 2. Based on the presence of charcoal fragments within the deposit (Sun et al., 2017), the outcrop at XGFSL at least contains the Phase 1 flow unit. With the absence of outcrop stratigraphy, and given that Machida et al. (1990) discovered both comenditic and trachytic products within the Phase 1 flow, we cannot state with certainty that the pyroclastic flow deposit at site XGFSL also represents Phase 2 eruptive material. We also note that Machida et al. (1990) might have sampled reworked deposits (H. Wei, personal communication, September 1, 2022). Whether the Phase 1 flow contains trachytic pumice or not needs further investigation.

5 Proximal post-Phase 1 tephra deposits

There are still disputes over whether some pyroclastic fall deposits emplaced after Phase 1 belong to the ME or not. Therefore, we temporarily name them as post-Phase 1 tephra deposits, even though some of them are known to be from Phase 2. They are mostly studied at outcrops on the northern peak on the caldera rim and to the east of the caldera (Fig. 1). Conflicting arguments from previous studies are also mostly based on observations and samples from these sites. Stratigraphic features of the post-Phase 1 tephra deposits studied at these sites and elsewhere have rarely been correlated (e.g., Chen et al., 2016; Pan et al., 2017; Sun et al., 2017), and are thus reviewed separately here.

5.1 Post-Phase 1 tephra at the northern peak and to the east of the caldera

At the northern peak of the caldera, two dark-coloured trachytic tephra layers directly lie above the Phase 1 tephra (e.g., Chen et al., 2016; Sun et al., 2017). They are from Phase 2 of the ME (Chen et al., 2016; Sun et al., 2017; Pan et al., 2017). To the east of the caldera, Machida et al. (1990), Sun et al. (2017), and Pan et al. (2020) found well-bedded tephra layers (Fig. 1), i.e., the post-Phase 1 tephra, lying above the Phase 1 tephra fall or flow deposit. At some outcrops, the Phase 1 and post-Phase 1 tephra are separated by a unit of non-pyroclastic or reworked pyroclastic deposit, taken to suggest a hiatus between Phases 1 and 2 of the ME (Machida et al., 1990; Sun et al., 2017; Zhao et al., 2020; Pan et al., 2020).

The post-Phase 1 tephra deposits to the east of the caldera are characterized by alternating colour (black to dark gray, yellow, and white) and grain sizes (fine ash to lapilli and even bombs). In most cases, no non-pyroclastic deposits are present in between these tephra layers. The only exception is at outcrop YC of Sun et al. (2017) (Fig. 1d; 30 km east of the caldera) where a mud layer was found in between these tephra units. We note here that YC of Sun et al. (2017) and YC of Pan et al. (2017) are two different locations. Throughout the text, YC refers to the site YC of Sun et al. (2017) unless specified otherwise.

Identifying Phase 2 tephra For outcrops to the east of the volcano (excluding YLW and DFH from Zhang et al. (2022a,b), which are more to the northeast and display limited stratigraphic features), if we assume that the tephra layer that directly lies above the Phase 1 eruptive products is trachytic in composition and shows no signs of reworking, it is likely that the deposit is from Phase 2. This is because the Phase 2 trachytic ash was dispersed to the east and even reached Japan, and it thus should be preserved at outcrops to the east of the caldera.

5.1.1 An alternative eruptive products correlation

Re-examining the stratigraphy and compositional data of the post-Phase 1 tephra units to the east of the caldera reported in Machida et al. (1990); Sun et al. (2017); Chen et al. (2016) prompts us to propose an alternative correlation of post-Phase 1 tephra deposits at sites SMFD, YC (of Sun et al., 2017), and DYT in their works. These sites are marked in Fig. 1 with the stratigraphic columns and compositions presented in Figs. 1 and 3.

Sites SMFD and YC Four pyroclastic units were discovered at site SMFD, 24 km east of the caldera. Above SMFD-1, which is from Phase 1 of the ME, there are three post-Phase 1 tephra fall units (the uppermost unit, SMFD-4 is interpreted as a fall deposit here which is consistent with Sun et al. (2017)). At YC of Sun et al. (2017), 30 km east of the caldera, above the YC-1 tephra unit from Phase 1, a mud-enriched layer (YC-2) underlies several bedded post-Phase 1 tephra fall units (YC-3, 4, 6, 7) and a mud layer (YC-5; Fig. 1f). According to Sun et al. (2017), YC-3, the basal post-Phase 1 tephra correlates with SMFD-4, the uppermost tephra layer there. It was suggested that the two correlated units were from a post-ME eruption based on age data given therein. This correlation and interpretation are unlikely, because they imply that Phase 2 tephra were not deposited at site YC of Sun et al. (2017) (as YC-3, the oldest tephra layer after Phase 1 there, was identified as post-ME in their work). This is counter to what we know about the Phase 2 tephra: (1) the Phase 2 trachytic tephra were dispersed to the east, reaching the Sea of Japan and Japan; (2) sites SMFD and YC are to the east of the caldera, and are only $\sim$ 10 km from each other (Fig. 1); (3) no signs of erosion have been reported at the two sites as well as other outcrops to the east of the caldera. Based on these lines of evidence, we know that the Phase 2 tephra are highly likely to be deposited and preserved in proximal outcrops (including YC) to the east of the caldera. Indeed, this has been confirmed in other studies (e.g., Machida et al., 1990; Pan et al., 2017). The previously-proposed unit correlation contradicts the arguments listed above, implying that YC-3 and SMFD-4 are not correlated. We propose instead that YC-3 and SMFD-2 (trachytic in composition), the two oldest post-Phase 1 tephra units at the two sites, are more likely to be correlated (Fig. 3).

Site DYT At outcrop DYT, $\sim$ 41 km east of the source vent, the basal tephra layer DYT-2 (overlying peat sediment DYT-1), comenditic in composition, was identified as post-ME tephra and correlated with YC-6 by Sun et al. (2017). This is unlikely since it implies that the comenditic Phase 1 tephra is absent at DYT. This contradicts the following observations: (1) the Phase 1 tephra were found as the basal tephra unit at all outcrops by Machida et al. (1990); Sun et al. (2017); Pan et al. (2017) to the east of the caldera. The Phase 1 tephra were mainly dispersed to the east and reached Japan. In particular, at Location 12 of Machida et al. (1990), $\sim$ 5.5 km west of site DYT, thick laminated Phase 1 tephra have been observed (Fig. 1); (2) isopachs of Phase 1 tephra constructed in previous works (Machida et al., 1990; Horn and Schmincke, 2000) suggest that the Phase 1 tephra were deposited at outcrop DYT (Fig. 6c); (3) no signs of erosion were reported at DYT. We therefore propose that DYT-2 corresponds to Phase 1 of the ME (Fig. 3).

5.1.2 Post-Phase 1 tephra age to the east of the volcano

Our arguments above suggest that radiocarbon dates for the post-Phase 1 tephra units to the east of the caldera are inconsistent with their stratigraphy, and the age data thus cannot support the presence of post-ME eruptive products to the east of the caldera as argued in previous works. As a result, for these sites, the only evidence that could potentially help determine whether post-ME eruptions occurred are stratigraphic

features. Among all outcrops to the east of the caldera, there is only one outcrop that has a well-defined mud layer (YC-5; Sun et al., 2017) preserved in between post-Phase 1 tephra units (Fig. 1d). It suggests the possibility of a hiatus in between the deposition of post-Phase 1 tephra units. At the same time, there are four outcrops within $<\sim$ 10 km from site YC of Sun et al. (2017) where such a mud layer has not been reported, suggesting a localized phenomenon. More detailed study on this site is needed.

Post-Phase 1 tephras to the east of the caldera underlie paleosol at some outcrops (e.g., YC of Pan et al., 2017; Fig. 1e), suggesting that the time from the last tephra deposition to now allows for soil development. Except for the mud layer (YC-5) observed by Sun et al. (2017), the absence of such a unit or any other evidence of a hiatus (e.g., reworking or erosion) within the post-Phase 1 tephra units to the east of the caldera supports the absence of eruptive products from post-ME eruptions there. It is thus more likely, and hence assumed in the rest of the text that all post-Phase 1 tephra to the east of the caldera are from Phase 2. This is consistent with Pan et al. (2017) and Pan et al. (2020). Whether eruptive products from post-ME eruptions are deposited to the east of the caldera assuming that post-ME eruptions exist, is a question that is different from whether post-ME eruptions exit. The latter will be discussed later in the text.

5.1.3 Disputes on the presence of comenditic material within the Phase 2 tephra units

Compositions of the Phase 2 tephra to the east of the caldera are inconsistent in previous studies, but it is unclear whether the samples are all from the same sub-layer (i.e., individual tephra layers within Phase 2 tephra). Pan et al. (2017) and Pan et al. (2020) found all Phase 2 tephra units to be trachytic, while Machida et al. (1990) and Sun et al. (2017) found both trachytic and comenditic pumice in Phase 2 tephra layers (Figs. 2e and 3). The compositional data from Machida et al. (1990) and Sun et al. (2017) are based on two different locations with consistent stratigraphy. They are Location 11 in Machida et al. (1990) and outcrop YC in Sun et al. (2017), which are about 30 km east of the caldera and $\sim$ 4 km from each other (Fig. 1). Both studies found that (1) in between the lowermost and uppermost Phase 2 tephra layers, there is at least one well-layered comenditic tephra unit (E6 in Machida et al., 1990 and YC-6 in Sun et al., 2017); and (2) the uppermost tephra units at the two sites contain both comenditic and trachytic tephra (E7 in Machida et al., 1990 and YC-7 in Sun et al., 2017; Fig. 3). Similar observations are also made at site DYT (i.e., DYT-3 and DYT-4 are characterized by bimodality in silica content; Fig. 2b by Sun et al., 2017), but its stratigraphy was not reported.

Reworking could explain the admixture of Phase 1 and 2 tephra, but it is difficult to explain the presence of a well-defined comenditic tephra layer that is within the Phase 2 tephra units. We suggest that comenditic tephra deposits might have been produced during Phase 2, but further studies will be required to confirm the matter either way. The Phase 2 tephra layers to the east of the caldera are composed of multiple tephra units, representing multiple eruption pulses. Their extents could differ, and it is possible that comenditic ash layer(s) may not cover some sample sites, possibly explaining why some studies did not find comenditic tephra within the Phase 2 fall deposits.

Based on the compositional data of Machida et al. (1990); Chen et al. (2016); Sun et al. (2017) and arguments above, we tentatively update unit correlation for Phase 2 tephra deposits to the east of the caldera (red lines marked in Fig. 3). The correlation is based on whether the sampled pumice contains solely comenditic or trachytic material, or a combination of the two. We put forward a unit correlation as a hypothesis, based on all available data, with the hope that future field studies will bring clarification.

5.1.4 Alternating coarse and fine tephra layers to the east of the caldera

Phase 2 tephra layers to the east of the caldera are characterized by alternating coarse and fine grain sizes (Machida et al., 1990; Pan et al., 2017; Sun et al., 2017; Pan et al., 2020). The contacts of these layers are not gradual, implying that a pair of coarse and fine layers were possibly not from a single eruption pulse. This is noteworthy as if that is the case, the fine tephra layers might be the fine co-ignimbrite ash elutriated and then deposited during and after the emplacement of the pyroclastic flow and surge deposits, respectively. Together with features of Phase 2 pyroclastic flow deposits that will be introduced below, it is likely that the coarser layers were from unsustained plumes with frequent column collapses or from frequent small pulsatory eruptions during Phase 2 (less likely for the latter as the flow deposit indicates frequent column collapses). The origin of the fine tephra layers, namely whether they were from the unsustained plumes or are co-ignimbrite ash generated from elutriation during pyroclastic flow and surge emplacement, needs more detailed study in the future.

5.2 Post-Phase 1 tephra at other outcrops

Horn and Schmincke (2000) suggested that Phase 2 produced dark-coloured trachytic agglutinates mantling the inner crater walls. Within the caldera, Pan et al. (2017) observed black scoria overlain by well-bedded pyroclastic materials with alternating grain sizes and colour (Point 2; Fig. 1). Compositions of the pumice there are similar to Phase 2 eruptive products observed to the east of the caldera, and are hence identified accordingly (Pan et al., 2017). Ramos et al. (2016, 2019) suggest that some post-Phase 1 tephra within the caldera are post-ME, but stratigraphic positions of their samples are not given (sample sites provided in their works), making it difficult to compare them with other studies.

At site 08-12 of Zhao et al. (2020), ∼1.5 km west of the western caldera rim (Fig. 1), the outcrop includes a unit of agglutinated bombs and pyroclastic material with parallel bands sandwiched by dark-gray brecciated tuffs and welded tuffs. These features suggest that they are Phase 2 eruptive products (Tables 1 and 2), and confirm that Phase 2 produced agglutinates (Horn and Schmincke, 2000). The stratigraphic position of the agglutinates also implies that they are not the oldest Phase 2 eruptive product.

5.2.1 Critical but poorly-studied outcrops for the Phase 2 tephra

At outcrops in valleys to the south of the caldera, massive and thick pyroclastic flow deposits interbed several to more than ten laminated pyroclastic deposit layers. The laminated layers have been identified as tephra layers and briefly described in Liu et al. (1998). If that is the case, as the Phase 1 tephra and flow deposits do not interbed each other, the flow and tephra deposits at such sites are definitely from Phase 2. The presence of multiple ash layers within the flow deposit is consistent and thus possibly correlated with the presence of multiple Phase 2 tephra layers to the east of the caldera.

Alternatively, these laminated layers within the pyroclastic flow deposit have been recently proposed as the result of vapor-phase alteration of ignimbrites (H. Wei, personal communication, September 1, 2022). So far, such outcrops have been poorly-studied. Future work is necessary to confirm the origin of these laminated layers.

5.2.2 A more comprehensive eruptive history of Phase 2

The stratigraphy of Phase 2 eruptive products introduced above suggests an eruptive history of Phase 2 that has been rarely elicited: it produced agglutinates that were only deposited within and near the caldera

rim (Horn and Schmincke, 2000; Pan et al., 2017; Zhao et al., 2020), pyroclastic flow and surge deposits, tephra from non-sustained plumes characterized by frequent column collapses, and possibly co-ignimbrite ash. Their sequence is not well-constrained, but will be critical for reconstructing the ME eruptive history for future works.

6 Proximal Phase 2 pyroclastic flow deposit

The Phase 2 pyroclastic flow deposit is dark-coloured, partially welded, and composed of fine-grained trachytic pumice and glass shards with lithics (Table 2; Machida et al., 1990; Horn and Schmincke, 2000). It has a much smaller extent compared to the Phase 1 pyroclastic flow (Machida et al., 1990; Horn and Schmincke, 2000; Zhao et al., 2020). No carbonized wood was found within the Phase 2 flow (Machida et al., 1990).

In most valleys 10-20 km from the centre of the caldera, Zhao et al. (2020) observed dark-coloured, welded, and thick pyroclastic flow deposits characterized by columnar jointing and the presence of lithic-rich and pumice-rich layers (lenses). Whether these deposits were from Phase 1 or 2 of the ME was not specified in Zhao et al. (2020), but their features and absence of charcoal suggest a Phase 2 origin. Extent and composition of the Phase 2 pyroclastic flow are subject to different interpretations.

6.1 The Phase 2 flow extent

The extent of the Phase 2 pyroclastic flow deposit was delineated by Horn and Schmincke (2000), who identified deposits in paleovalleys mainly to the south along the Yalu River but also to the north. Zhao et al. (2020) investigated facies of the ME pyroclastic flow deposits, but identifying the phase of the flow deposits was not their main objective. They mapped the overall extent (i.e., union of Phases 1 and 2) of the ME flow deposits in the Chinese territory. The extent is roughly composed of two fan-shaped lobes with one to the northeast and the other to the west (Fig. 1). Zhao et al. (2020) described and categorized the ME flow deposits based on distance, volcano topography, and their stratigraphic features: pyroclastic flow deposits within 0-20 km from the caldera are dark-coloured, welded, and found in stream gullies and valleys with the absence of carbonized wood; the flow deposit beyond this distance is mainly composed of loose grey and grey-white pumice. It contains carbonized wood, and its distribution is fan-shaped (Fig. 1). These features suggest that flow deposits within 0-20 km of the caldera centre were likely from Phase 2, while more distant flow deposits from Phase 1. If this is true, Zhao et al. (2020) confirm that the Phase 2 flow extent is strongly controlled by topography, and has a broader extent compared to its extent inferred by Horn and Schmincke (2000): they are not only distributed along paleovalleys to the south and north of the caldera, but also along valleys to the west and northeast of the caldera. It is possible that the Phase 1 flow deposit underlies that of Phase 2 within 20 km from the caldera centre, but is not exposed at the studied outcrops. In other words, in the direction where the Phase 1 flow deposit is found distally, it must underlie the Phase 2 flow deposit proximally.

6.2 Uncertainty on the Phase 2 flow composition

Similar to the Phase 2 tephra to the east of the caldera, pumice composition within the Phase 2 pyroclastic flow is subject to uncertainty. Machida et al. (1990) found both comenditic and trachytic pumice within the Phase 2 flow (Fig. 2e). In addition to site XGFSL introduced before, Sun et al. (2017) also studied pumice from the ME flow deposits at sites LFZ (∼15 km northeast of the caldera), NTC (∼35 km north

of the caldera), and JJ (∼13 km southwest of the caldera), but they did not identify whether the sampled deposits were from Phase 1, 2, or both. Samples from the first two sites show bimodality (i.e., comendite and trachyte) in their silica content, and the ones from JJ are uniformly trachytic (Fig. 2). It is not certain whether comenditic pumice was present and if so, what its abundance was in the Phase 2 flow deposit.

7 Distal B-Tm ash

The layered (defined as equivalent of non-crypto tephra in this work) B-Tm ash was mainly dispersed towards the east, and can be found in sediment cores from the Sea of Japan and Japan (Furuta et al., 1986; Machida et al., 1990; Nanayama et al., 2003; Okuno et al., 2011; Derkachev et al., 2019; McLean et al., 2020; Figs. 4 and 5). For the layered B-Tm ash, its northernmost extent is in the south of Lake Kushu, Japan (∼1100 km east-northeast of the caldera) where B-Tm cryptotephra was found (Chen et al., 2016). Its southernmost extent is probably near Lake Suigetsu, Japan (∼990 km southeast of the caldera) where the tephra is a thin ash layer (< 1 mm; McLean et al., 2016). The B-Tm cryptotehra has also been discovered within marine core 13PT-P4 in the southwest of the Sea of Japan, about 580 km south-southeast of the source region (Fig. 4; Chen et al., 2022). To the west, the ash was found as cryptotephra within Maar Lake Sihailongwan, about 125 km west-northwest of the volcano (Sun et al., 2015, 2016). The B-Tm cryptotephra and trachyte grains were also found in ice cores in Greenland (Sun et al., 2014a). Compositionally, the B-Tm ash in most cases shows bimodality in its silica content, which corresponds to the comenditic and trachytic tephra from proximal sites. Distal B-Tm ash with silica content in between the two end members was also found at some sites (e.g., in the Sea of Japan and in Maar Lake Sihailongwan as shown in Fig. 5; Machida et al., 1990; Furuta et al., 1986; Sun et al., 2015).

7.1 Stratigraphic and spatial variation in composition

Compositions of the B-Tm ash at sites far from the caldera (> 100 km from the vent) are given in Figs. 4 and 5. Due to the thinness of the B-Tm ash, only a few studies analyzed whether it has compositional variation with respect to stratigraphy. At site/core KH69-2-23 (JS4), ∼530 km east of the volcano, the lower unit of the B-Tm ash is dominantly comenditic, the middle unit is characterized by a range of silica content (SiO_2 ranges from $\sim 66-75\%$), and the upper unit shows bimodality in the silica content (Fig. 5e; Machida et al., 1990). In Lake Sihailongwan, about ∼ 125 km west of the volcano, B-Tm cryptotephra were found (Sun et al., 2015). Samples from the depth of 53-cm contain both comenditic and trachytic glass shards, and samples from the depth of 52-cm are dominantly trachytic with only one comenditic glass shard (Fig. 4i and j).

In most distal sample sites, both comenditic and trachytic glass shards can be found within the B-Tm ash. The exceptions are (1) at Lake Suigetsu, central Honshu, Japan and at core 13PT-P4 in the southwest of the Sea of Japan, where the sampled B-Tm glass shards are almost all comenditic (with only a few shards with lower silica content as seen in Fig. 4g and h; McLean et al., 2016; Chen et al., 2022). The comenditic ash (which is likely to be Phase 1 based on previous studies; McLean et al., 2016) was dispersed more to the south compared to the trachytic ash (McLean et al., 2016; Chen et al., 2022); (2) and at sample sites in Primorskii krai, Russia, the B-Tm ash glass shards are dominantly trachytic (Razjigaeva et al., 2020). The latter suggests that limited comenditic ash was dispersed to the east-northeast, consistent with proximal Phases 1 and 2 tephra thickness distributions (Pan et al., 2020).

The B-Tm ash has been sampled and analyzed along the coast of southern Hokkaido by Nakanishi et al. (2020). The sample sites are marked as squares with compositional data given in Fig. 4. The glass shard compositions do not change spatially at these sites.

Although the B-Tm ash has been sampled and studied at many distal sites, it is still difficult to construct extents of the B-Tm ash from Phases 1 and 2 separately. In fact, Machida et al. (1990) hypothesized that the majority of the B-Tm ash, including the comenditic ash, was from Phase 2 of the ME. This was supported by the similarity in lithology and composition between the uppermost Phase 2 tephra at proximal sites and the distal B-Tm ash analyzed in their work. They stressed that the proposition stayed at a hypothetical level, and their proximal samples might have been reworked (H. Wei, personal communication, September 1, 2022), but we did not find any studies that attempted to test their hypothesis.

McLean et al. (2016) proposed the possibility that the B-Tm ash contains co-ignimbrite ash from the ME. As mentioned earlier, this is supported by the presence of co-ignimbrite ash at proximal sites.

We also stress here the necessity of interpreting the layered and cryptotephra B-Tm ash thickness separately. The tephra grains within the two are subject to transport processes at very different time scales and (or) potentially reworking for the cryptotephra. For example, cryptotephra is not-layered and preserved with other types of deposits, suggesting that it took much longer time for the corresponding tephra grains to deposit or that the cryptotephra has been reworked. Interpretations that do not differentiate the two (i.e., layered tephra and cryptotephra) could be misleading. For example: the B-Tm cryptotephra thickness is often defined as the thickness of a sediment section that has B-Tm tephra grains per unit volume greater than a certain threshold. If such cryptotephra thickness is treated equally as the layered B-Tm ash thickness, the B-Tm ash volume and extent would be significantly overestimated.

8 Critical and open questions associated with the ME

The eruptive history of the ME remains only partially understood. The uncertainty partially derives from the disputes and uncertainty introduced above. Additionally, sometimes the assumptions that support certain interpretations have been updated or better characterized, but the corresponding interpretations are left unmodified. We must inherit not only conclusions but also the supporting evidence from previous works for future studies of the ME. In this section, we discuss critical and open questions associated with the ME eruptive history in the hope they will be useful in stimulating future studies.

8.1 Whether post-ME eruptions exist

We have shown that with one exception (Sun et al., 2017), no stratigraphic observations imply post-ME eruptive products to the east of the caldera, supporting the arguments of Pan et al. (2017). However, this does not negate the possibility of post-ME eruptions, because it is possible that post-ME eruptions occurred and had their eruptive products deposited at other locations. Ramos et al. (2016, 2019) argue for post-ME eruptions based on samples within and near the northeastern rim of the caldera, though the stratigraphic positions of their samples were not specified. On the other hand, Pan et al. (2017) suggest that trachytic deposits that were once thought to be post-ME are primary or reworked deposits of the ME. We believe this remains a critical question for future work: what was the post-ME eruptive history, if any? Many aspects remain unknown or unexamined. For example, if post-ME eruptions occurred, their eruptive products characteristics (e.g., extent and grain size) should match their eruptive styles, and their ages need to be consistent with the stratigraphy. The difficulty of fully resolving this question highlights the importance

of spatially correlated pyroclastic deposit stratigraphy within and near the caldera, which is still currently unavailable.

Historical accounts have been examined for testimonies of post-ME eruptions, but as noted in Pan et al., 2017, their interpretation is fraught with difficulty due to their ambiguous nature.

8.2 Proximal Phases 1 and 2 tephra thickness distributions

Isopachs of proximal ME tephra have been constructed in Liu et al. (1998) and Horn and Schmincke (2000). The former shows the overall thickness distribution and is given in Fig. 6c. It was used to constrain the maximum tephra volume of the ME in Yang et al. (2021). Isopachs of Horn and Schmincke (2000) characterize the Phase 1 tephra.

New local isopachs of the ME tephra to the east of the caldera are plotted, and observed thicknesses are compared with isopachs constructed in previous works (Fig. 6). We have shown previously that the newly observed ME comenditic tephra to the northeast of the caldera might be from either Phase 1 or 2. With these observations excluded, comparison in Fig. 6c and d suggests that the northern extent of the Phase 1 tephra constructed in Machida et al. (1990) is consistent with its most recent thickness observations, whereas the northern extent of the Phase 2 tephra (Fig. 6b) constructed in their work needs to be updated and should be farther north.

8.3 Eruption volume

Volume ranges of the ME eruptive products are estimated in Yang et al. (2021). The B-Tm ash and proximal tephra volume ranges contribute to the greatest uncertainty (27-63 and >4.2-23 km^3). It is hard to further constrain their volumes due to the limited sample sites in the DPRK' s territory and the difficulty of differentiating the Phases 1 and 2 tephra for the distal B-Tm ash. Nonetheless, contradictory to some prior studies, it is clear now that the Phase 2 tephra volume is significant. This is because the proximal thickness of the Phase 2 tephra to the east and northeast of the caldera is comparable or even thicker than that of the Phase 1 tephra (Fig. 6), and the trachytic B-Tm ash from Phase 2 has been observed in most sites in the Sea of Japan and Japan. Improved determination of the masses of both Phase 1 and 2 deposits will be important for estimation of the volatile yields to the atmosphere on eruption of each phase, since the two magmas can be expected to have different carrying capacities for sulfur and other volatile species of interest.

8.4 Other eruption source parameters

Other eruption source parameters (e.g., column height and mass eruption rate) of the ME have been estimated in Liu et al. (1998); Yu et al. (2013), and are all based on isopachs and isopleths constructed in Liu et al. (1998). The estimation of other eruption source parameters also relies on assumptions that can be potentially updated in future studies. For example, the eruption duration, excluding the hiatus between the two phases, was estimated to be 111-333 hours by Liu et al. (1998), which was based on several assumptions, including the pyroclastic flow deposit being a 7.47 m-thick flat disk with a radius of 40 km, a total tephra volume of $\sim$ 83 km^3, and a mass eruption rate of $1*10^8-3*10^8$ kg/s. The pyroclastic deposit volumes have been updated (Horn and Schmincke, 2000; Zhao et al., 2020; Yang et al., 2021), and the assumed mass eruption rate is consistent with other eruptions with similar magnitude (e.g., $2*10^9$ kg/s for the 1815 Tambora eruption Kandlbauer and Sparks, 2014 and 10^8-10^9 kg/s for the Pinatubo eruption; Koyaguchi and Tokuno, 1993;

Holasek et al., 1996). With our improved understanding of the complicated eruptive history of the ME, its eruption source parameters need to be re-estimated separately for the two phases in future work.

8.5 Eruption hiatus

At some sites to the east of the caldera, (possibly reworked) pyroclastic or non-pyroclastic materials were observed in between Phases 1 and 2 eruptive products. They indicate the presence of a short depositional hiatus between Phases 1 and 2 and are described differently in previous studies, such as a very thin and immature soil-like bed (location unspecified; Machida et al., 1990), mud-enriched layer (sites SMFD and YC; Sun et al., 2017), and coarse, poorly-sorted, matrix-supported volcaniclastic materials rich in soil with a thickness of > 3 m (site HSG; Pan et al., 2020). The B-Tm ash layer observed in Japan does not contain a well-defined unit of non-tephra material. This is likely due to the low sedimentation rate of the corresponding depositional environments (Pan et al., 2020), or less likely but possibly related to the hypothesis of Machida et al. (1990) that all B-Tm ash was from Phase 2 of the ME.

The duration of the hiatus is poorly constrained. Two different historical records in Japan both indicate that on February 3rd, 947 CE, three months after the beginning of the ME, there was a sound in the sky that resembled thunder (Hayakawa and Koyama, 1998). It is tentatively hypothesized to be linked to the Phase 2 of the ME. Nonetheless, we argue here that a three-month hiatus has difficulty in explaining the aforementioned B-Tm cryptotephra stratigraphy at Maar Lake Sihailongwan (i.e., combination of trachytic and comenditic glass shards at 53-cm depth of the core and dominantly trachytic glass shards at 52-cm of the core; Fig. 5i and j). The cryptotephra samples there are preserved within varved maar lake sediments. Sediments comprising annual laminated layers are well developed in this area (Sun et al., 2015). The maar lake is fed primarily by groundwater inflow and rainfall during summer with no outlets for stream transportation (Liu et al., 2005). A three-month hiatus during winter at the latitude of 42.28° would be short to generate the observed tephra compositional variability. Closer to the caldera, a three-months hiatus during winter is also difficult to explain the presence of mud-enriched layer or thin and immature soil-like bed between Phases 1 and 2 eruptive products observed in previous studies. The question of the hiatus is an important one for further study.

8.6 Eruptive style and plume dynamics

Pan et al. (2020) found lacustrine deposits on the western slope of the northern outlet of the caldera lake which were ∼100 m above the current caldera lake level. This was taken to suggest the presence of a (caldera) lake prior to the ME. If so, water-magma would likely have played a role in the ME, but this has been poorly investigated so far. Phase 1 of the ME was characterized by a widespread fall deposit followed by the emplacement of pyrocalstic flow deposit. For Phase 2, we know that it produced agglutinates that were dispersed locally near the caldera rim and alternating tephra and pyroclastic flow (and likely co-ignimbrite ash) deposits from unsteady plumes. It is likely that the transition between the two was related to water-magma interaction and partial caldera collapse after Phase 1. The role of water-magma interaction during the ME needs further investigation. Critically, observations of the base of the ME deposits would greatly help in identifying this interaction and also further constraining the eruptive volume.

In sharp contrast to the Phase 1 flow, the Phase 2 pyroclastic flow deposit is mostly distributed along stream gullies and valleys near the caldera, suggesting its emplacement was more strongly controlled by topography. This might be related to caldera collapse prior to Phase 2 and after Phase 1 which, if oc-

curred, could lower the caldera floor and make the emplacement of the Phase 2 flow deposit more subject to topography. Further studies of the dynamics of emplacement of the two deposits would be worthwhile.

9 Final remarks

In this work, we have re-examined different observations, arguments, and interpretations concerning the ME and putative post-ME eruptions. We have elaborated on why some points of contention in the scientific literature cannot be resolved based on available information. We have proposed several nuances in interpretation and proposed hypotheses and highlighted critical outcrops for future studies. We find that a universal stratigraphy for the ME (and putative post-ME eruptions) is still sorely needed, especially in the proximal range (<50 km), and the stratigraphy of outcrops to the west and to the southeast of the caldera (i.e., outcrops in the DPRK) remains little reported. This makes intercomparison between some works challenging because there is not a clear equivalence of stratigraphic usage. Our understanding of the distal B-Tm ash can be improved by more sample sites and more detailed study on its variation in stratigraphic features.

Based on our review, disputes over the ME, potentially post-ME eruptions, and their products can be summarized as:

- Comenditic tephra might have been produced during Phase 2 of the ME (e.g., Machida et al., 1990; Sun et al., 2017). For a new site, we need to use both composition and stratigraphy to determine which phase a given ME tephra layer corresponds to. We suggest that the ME comenditic ash reported from northeast of the volcano (Zhang et al., 2022b,a) could be from either Phase 1 or 2 of the ME rather than definitely Phase 1.

- The Phase 1 pyroclastic flow might contain trachytic material (Machida et al., 1990). This hypothesis has been neither validated nor rejected in later works.

- All tephra layers observed to the east of the caldera that overlie the Phase 1 comenditic tephra are likely to derive from Phase 2 of the ME, rather than post-ME eruptions. The only evidence against this argument is a mud layer in between tephra units at outcrop YC of Sun et al. (2017);

- Phase 2 of the ME may have produced both trachytic and comenditic products (Machida et al., 1990; Sun et al., 2017) rather than just trachytic material as assumed in some works. Outcrops in paleovalleys south of caldera are critical for future works given the poorly-studied stratigraphy there.

- Phase 2 eruptive products within and to the west and south of the caldera are not correlated well with the better-studied Phase 2 tephra units to the east of the caldera. Ramos et al. (2016, 2019) suggest that post-ME eruptions existed, but how their samples are correlated with pyroclastic deposits elsewhere remains uncertain. The post-ME record still needs to be established in future works with clearer evidence for any significant activity since the 10th century episode.

- Phase 2 of the ME produced agglutinates, alternating pyroclastic flow and fall deposits from non-sustained plumes characterized by frequent column collapses. The alternating coarse and fine Phase 2 tephra layers to the east of the caldera also possibly suggest the deposition of co-ignimbrite ash near the caldera, which needs to be tested in future works.

- It is difficult to construct extents and thickness distributions for the Phases 1 and 2 B-Tm ash separately, because limited stratigraphic and spatial compositional variation exist for the B-Tm ash. The

543 distal B-Tm ash contains trachytic glass shards, suggesting that the Phase 2 tephra are widespread,
544 and their volume is at least not negligible as assumed in some studies.

545 Better understanding of Changbaishan/Paektu-san Volcano's eruptive past is challenging to realize but
546 necessary, given the recent unrest, and fast pace of development in the region, as well as the wider cultural
547 significance of the volcano.

10 Tables

Table 1: General characteristics of proximal tephra fall and flow deposits from Phase 1 of the ME.

Unit	Reference	Description type	Components and their features
Phase 1 tephra	Machida et al (1990)	General description	Color: light colored Composed of highly vesicular silicic pumice together with small amount of basaltic fragment.
	Horn and Schmincke (2000)	General description	Color: white to gray Comenditic rhyolitic pumice: Moderately to highly vesicular (≥40% vesicles); Subangular and relatively equant; Crystal poor with 3 vol.% phenocrysts. Lithics: older basalt and trachyte of the stratocone and syenite; Rooted tree trunks are common in the deposit; Approximately 1% of the pumice lapilli contain dark bands of trachyandesite.
	Pan et al (2017)	Noticeable feature	Comendite pumice layer with minor but ubiquitous mingled comendite-trachyte pumice.
	Sun et al (2017)	Noticeable features	Dark gray to banded pumice lapilli and blocks can be found within the deposit; Lithics include traychyandesitic volcanic and granite clasts; Charcoal fragments and Larix leaves can be found at some sites.
Phase 1 flow	Machida et al (1990)	General description	Color: white to gray; Composed of light- and dark-colored pumice and glass shards, lithic fragments; Abundant carbonized tree trunks and banded pumice lumps; Overlie surge deposit at some outcrops.
	Horn and Schmincke (2000)	Noticeable features	Approximately 1% of the pumice lapilli contain dark bands of trachyandesite; Charcoal fragments are extremely abundant, entire, and generally carbonized tree trunks are common; Unwelded.
	Shi et al (2005)	Noticeable feature	Pumice of various colors which includes white, black, and gray.

Table 2: General and noticeable characteristics of proximal tephra fall and flow deposits from Phase 2 (post-Phase 1) of the ME.

Unit	Reference and description type	General description
Phase 2 tephra	Machida et al (1990); General description.	Alternation of gray pumice and ash layers; Comprised of four plinian pumice fall units and three ash fall units.
	Horn and Schmincke (2000); General description.	Emplaced as proximal agglutinates mantling the inner crater walls Composition: trachyte.
	Pan et al (2020); Site: HSG.	Multiple thin (~5-10 cm) normally graded layers characterize the trachytic ash deposit.
Post-Phase 1 tephra (identified as Phase 2 in this work)	Sun et al (2017); Site: YC.	Alternation of coarse and fine tephra layers; Identified as post-ME tephra in their work.
Phase 2 flow	Machida et al. (1990)	Dark-colored pyroclastic flow; Fine grained dark-colored pumice and glass shards with lithic fragments; No carbonized wood.
	Liu et al (1998); Site: valleys south of the caldera	Pyroclastic flow deposits interbed with several to more than ten tephra layers.
	Horn and Schmincke (2000)	Slightly welded pyroclastic flows (trachytic composition).

11 Figures

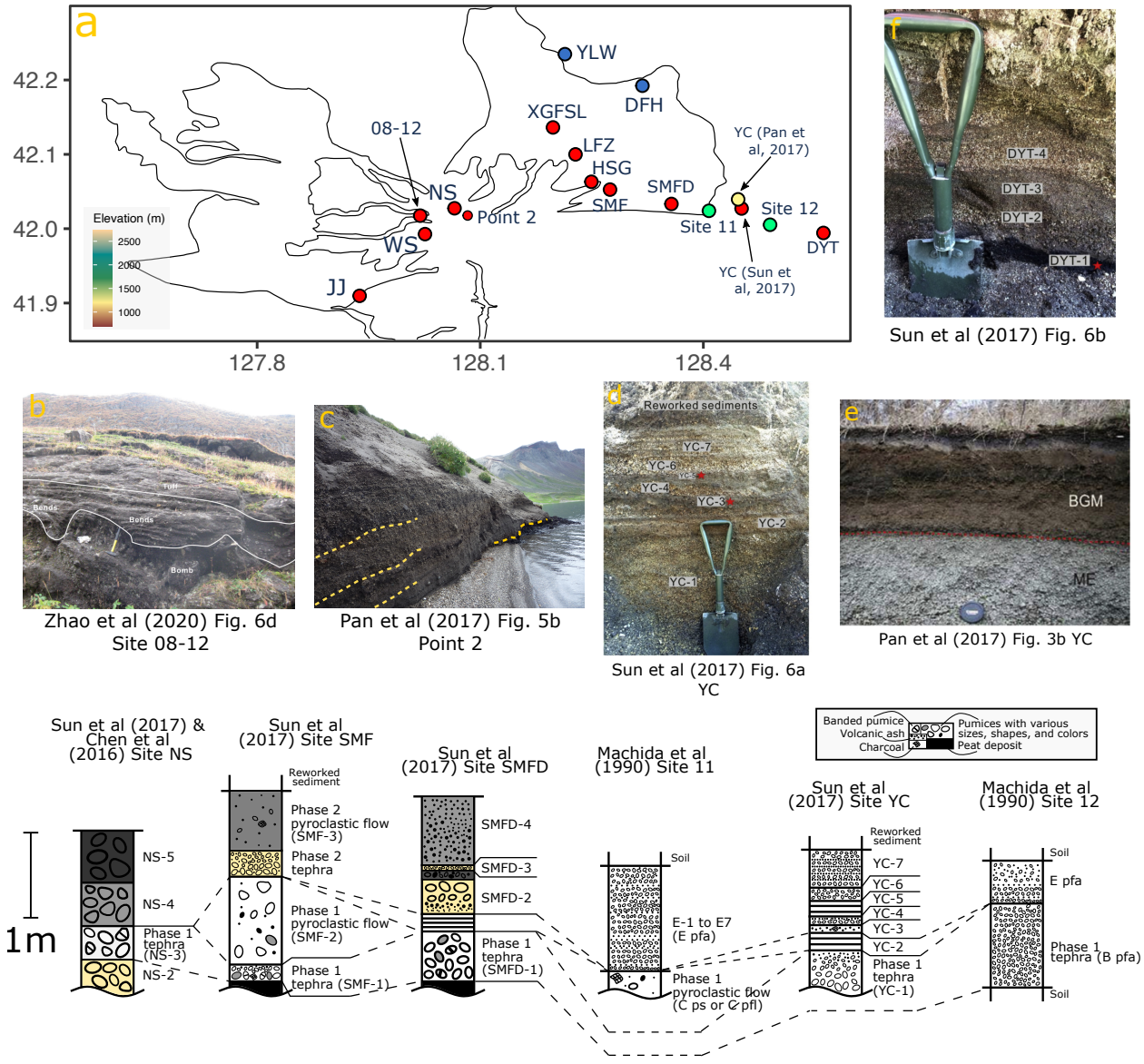

Figure 1: a: Elevation map of the Changbaishan/Paektu-san Volcano with sample sites marked. The solid line digitized from Zhao et al. (2020) delineates the mapped extent of the flow deposits from the ME in the Chinese territory. b-f: field pictures at different sample sites with references given. "BGM" in e refers to Phase 2 (Pan et al., 2017). The yellow dashed lines in c are added in this work to highlight different features of the outcrop. Stratigraphic columns below the field pictures are constructed based on descriptions from different works with references given. Dashed lines mark the unit correlation, which is based on proposition in this work. See text for detail. YC-2, YC-5, and the geological unit between SMFD-1 and SMFD-2 are mud-enriched or mud layer (Sun et al., 2017).

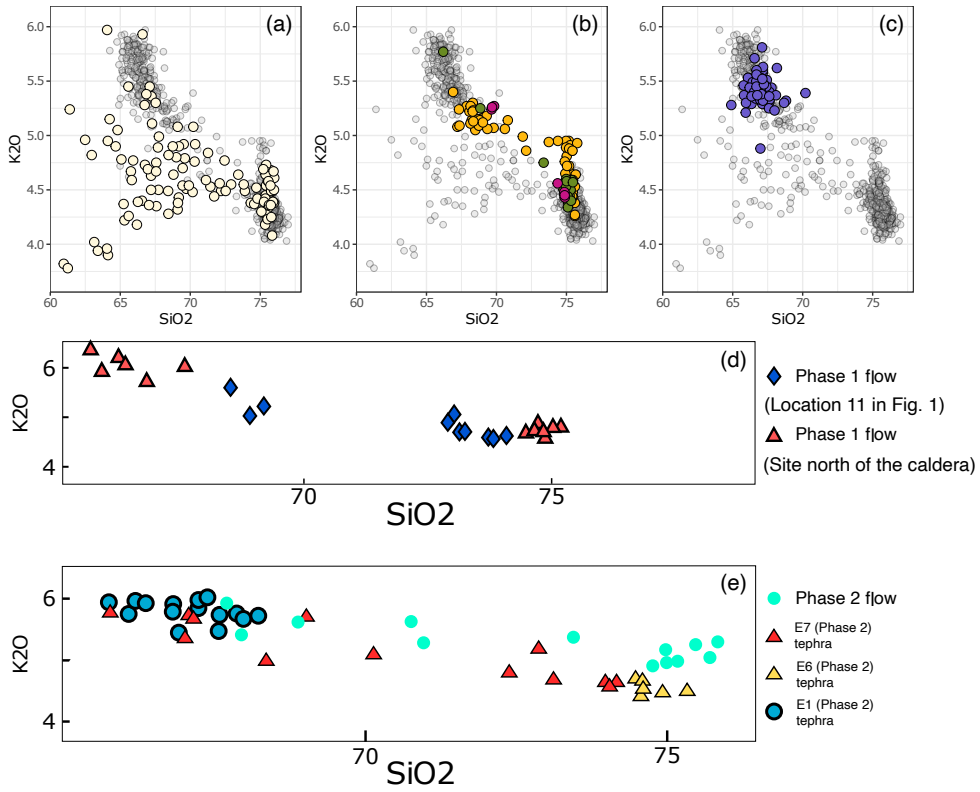

Figure 2: Glass shard compositional biplots (normalized to 100% for a-c) of banded pumice (a: sample sites near the caldera rim and SMFD; light yellow points) and pumice within pyroclastic flow units from the ME (b: yellow, green and magenta points correspond to samples from sites XGFSL, LFZ, and NTC; c: purple points from site JJ). Data in a-c are all from Sun et al. (2017). The transparent gray points in the background in a-c correspond to the complete dataset reported in their work. d and e: re-drawn Fig. 9A and B of Machida et al. (1990) showing the glass shard compositional variation of the proximal eruptive products of the ME.

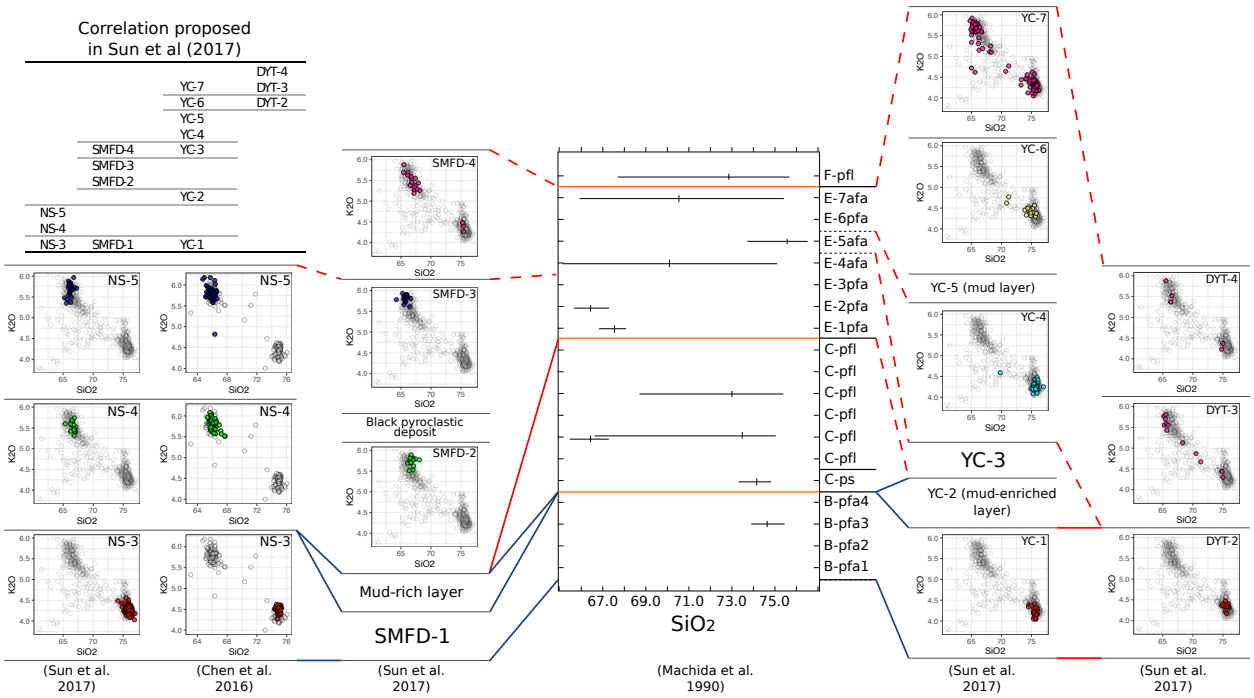

Figure 3: Glass shard compositional biplots (normalized to 100%) and SiO_2 content from Machida et al. (1990); Chen et al. (2016); Sun et al. (2017) with sample sites given. The table on the upper-left corner shows the unit correlation proposed in Sun et al. (2017). For the rest of the figure, blue solid lines between biplots represent correlation from previous works that do not need to be updated. The red lines denote the proposed unit correlation in this work. Correlation that cannot be established with a one-to-one correspondence are marked as red dashed lines. Point colors of the biplots do not imply any correlation. Light gray colored points in the background of each compositional biplot correspond to the complete dataset given in respective works. The SiO_2 content figure in the middle is modified from Fig. 7 of Machida et al. (1990), which shows silica contents of their samples. The B-pfa and E-1 to E-7 units correspond to fall deposits from Phases 1 and 2, respectively. The C-pfl and F-pfl units (C-ps corresponds to the surge deposit) correspond to Phases 1 and 2 pyroclastic flow deposits, respectively.

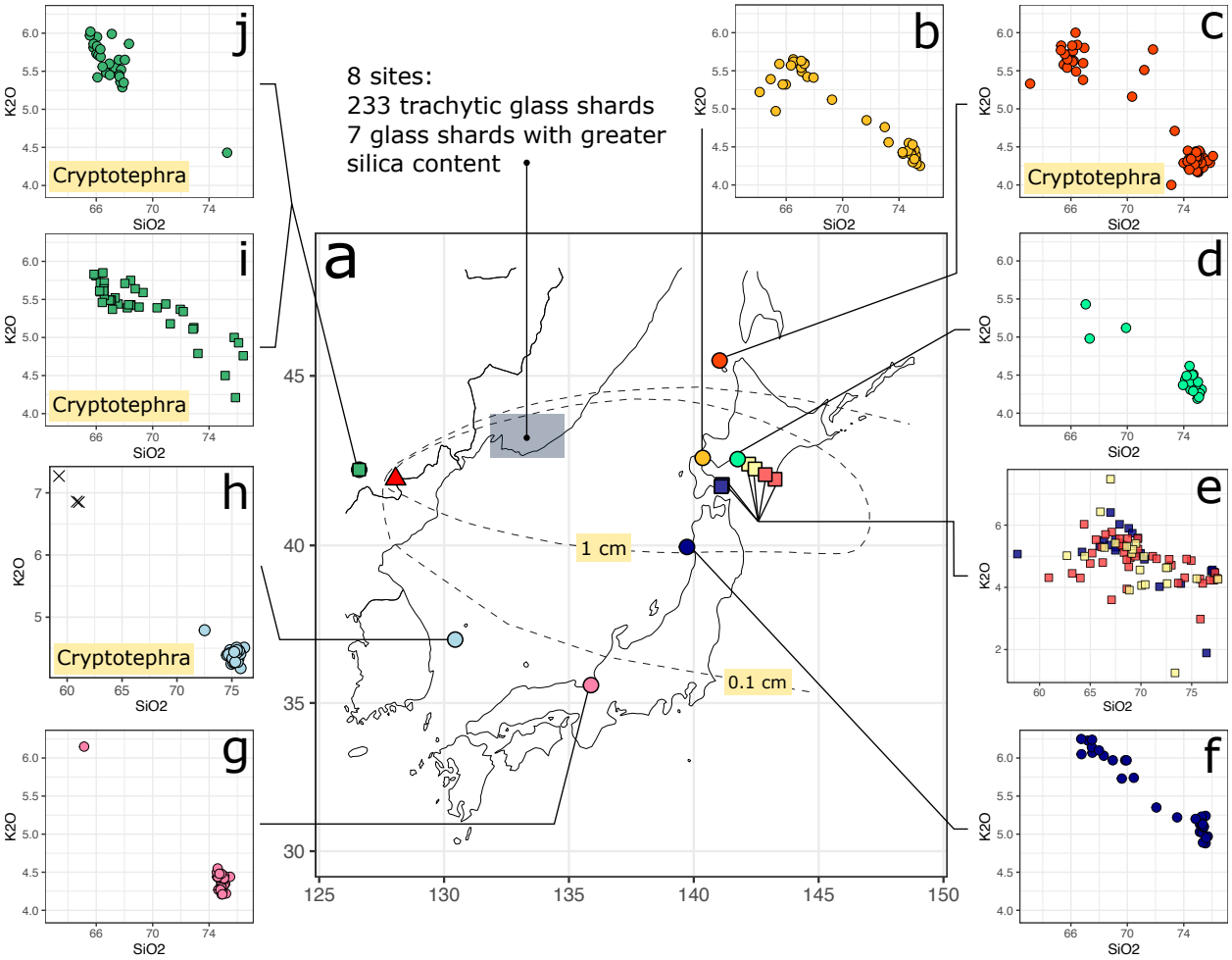

Figure 4: a: Sites in Sea of Japan and Japan with the B-Tm ash sampled for compositional analysis. b-j: glass shard compositional biplots (normalized to 100%) from different studies. b-j are from Hughes et al. (2013), Chen et al. (2016), McLean et al. (2016), Nakanishi et al. (2020), Okuno et al. (2011), McLean et al. (2016), Chen et al. (2022) (cross as outlier), Sun et al. (2015), and Sun et al. (2015), respectively. In e, it composes of samples from six sites marked as squares in a. Data in i and j are from cryptotephra samples from 53 and 52 cm depths, respectively, of the core in Lake Sihailongwan to the west of the caldera (Sun et al., 2015). The light blue box in (a) covers 8 sample sites in Russia with the B-Tm ash sampled, and there are 233 trachytic glass shards and ~7 glass shards with greater silica content sampled at these sites (Razjigaeva et al., 2020). The two dashed lines correspond to the 1- and 0.1-cm isopachs constructed in Yang et al. (2021).

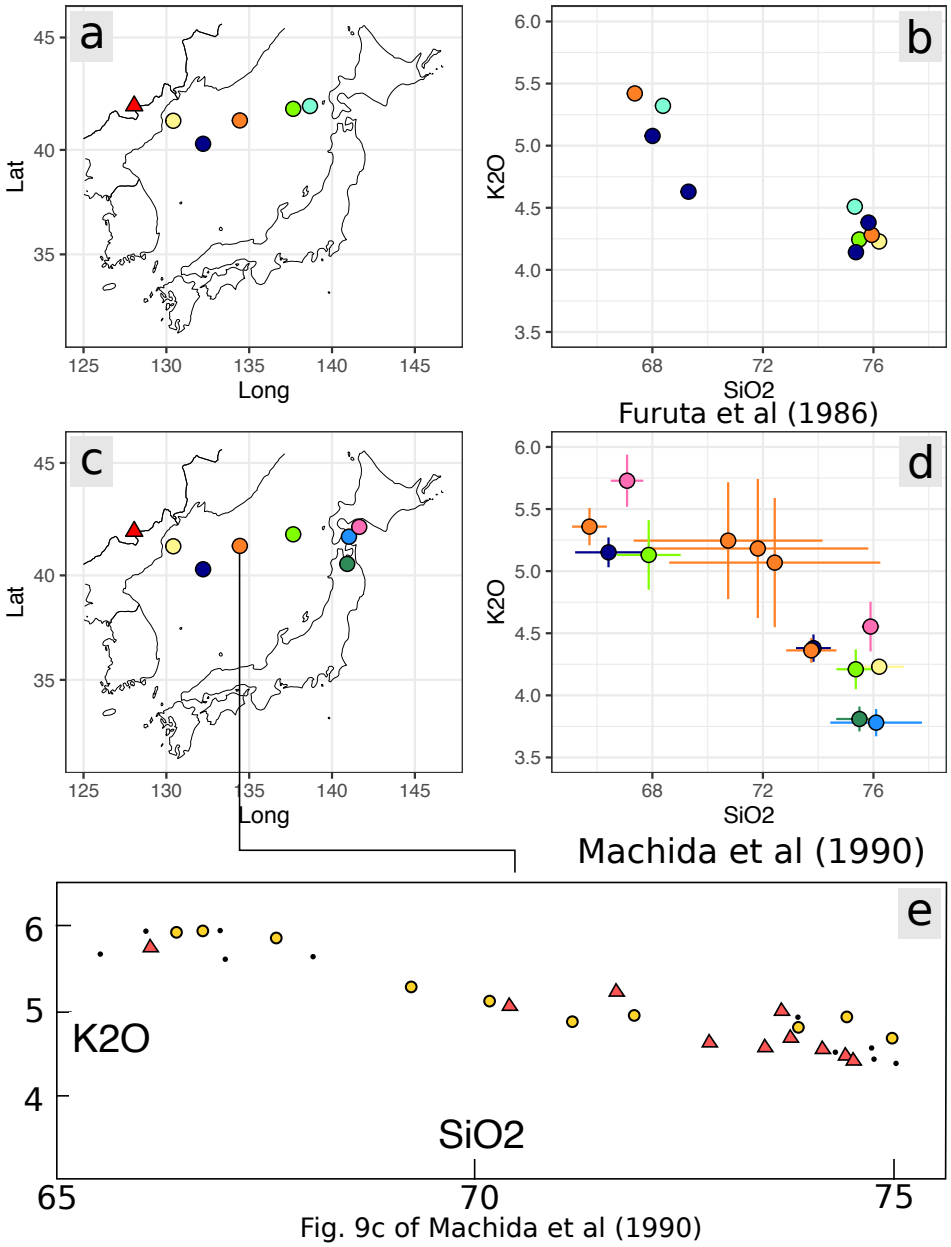

Figure 5: a and b: sample sites and compositonal biplots of the B-Tm glass shards from Furuta et al. (1986). No standard deviations are given in their work and the colors in a and b match each other. c and d correspond to sample sites and compositional biplots (normalized to 100%) of the B-Tm glass shards from Machida et al. (1990) with error bar given. Data in b and d are normalized. e is digitized from Fig. 9c of Machida et al. (1990) showing the individual glass shard measurements at the orange site in c (JS4 or KH69-2-23). Triangle, circle, and dots correspond to samples from the lower, middle, and upper units of the B-Tm ash within the core.

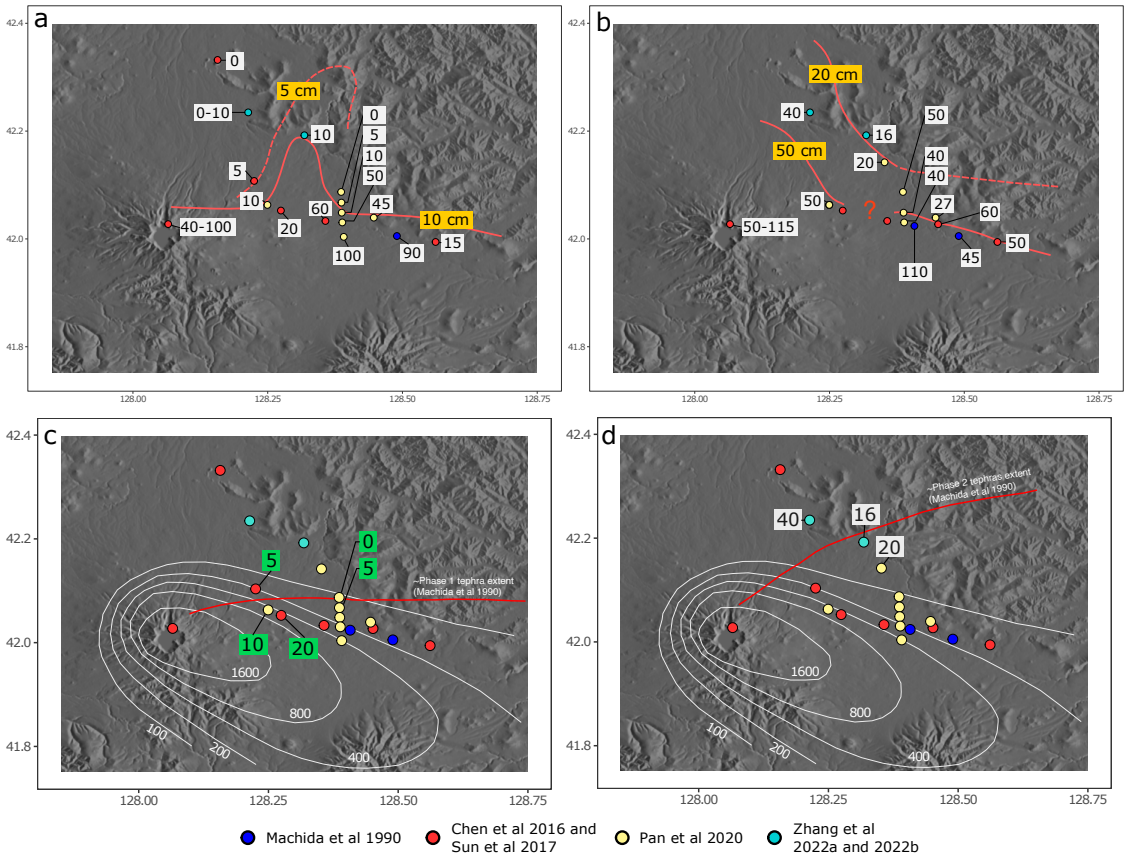

Figure 6: Thickness of basal comenditic ash (a; with comenditic ash thickness from (Zhang et al., 2022b,a) included) and summed thickness of Phase 2 ash layers (b) at respective outcrops with sample sites and references given. Note that the ash thicknesses with sites marked in light blue are from Zhang et al. (2022a,b). In b, thicknesses at the light blue sites are the thicknesses of the upper trachytic ash. Red lines in a and b correspond to isopachs constructed in this work (dashed lines are constructed with greater uncertainty). The 50-cm isopach in b is not connected because the Phase 2 ash thicknesses at the two red sites near the question mark are thick, but whether they are primary ash is uncertain. White lines in c and d correspond to the total ME tephra isopachs from Liu et al. (1998). Phases 1 (excluding comenditic ash thicknesses from Zhang et al., 2022a,b) and 2 tephra thicknesses near their respective northern extents given by Machida et al. (1990) are labeled. Only the upper trachytic ash is assumed as Phase 2 at sites of Zhang et al. (2022a,b) in d. All units in cm.

12 Acknowledgments

This is a synthesis of the work of others and we warmly acknowledge their many and varied contributions. Q. Yang, S.F. Jenkins, and G.A. Lerner were partly supported by the National Research Foundation Singapore and the Singapore Ministry of Education under the Research Centres of Excellence initiative (Project Number: NRF2018NRF-NSFC003ES-010), and comprises Earth Observatory of Singapore contribution number 474. G.A. Lerner and S.F. Jenkins were partly supported by funding from the AXA Joint Research Initiative under the project "Volcanic Risk Assessment in Asia". This work forms part of a jointly funded collaboration (NRF-NSFC) between Q. Yang, S.F. Jenkins, and G.A. Lerner at the Asian School of the Environment/Earth Observatory of Singapore at NTU and H. Wei, J. Xu, and B. Pan at the China Earthquake Administration.

References

X.-Y. Chen, S. P. Blockley, P. E. Tarasov, Y.-G. Xu, D. McLean, E. L. Tomlinson, P. G. Albert, J.-Q. Liu, S. Müller, M. Wagner, et al. Clarifying the distal to proximal tephrochronology of the millennium (b–tm) eruption, changbaishan volcano, northeast china. *Quaternary Geochronology*, 33:61–75, 2016.

X.-Y. Chen, S. P. Blockley, R. Fletcher, S. Zhang, J.-H. Kim, M.-H. Park, C. Chen, J. Yin, and Y.-G. Xu. Holocene tephrostratigraphy in the east sea/japan sea: Implications for eruptive history of ulleungdo volcano and potential for hemispheric synchronization of sedimentary archives. *Journal of Geophysical Research: Solid Earth*, 127(2):e2021JB023243, 2022.

A. C.-s. Cheong, Y.-J. Jeong, H. J. Jo, and Y. K. Sohn. Recurrent quaternary magma generation at baekdusan (changbaishan) volcano: New zircon u-th ages and hf isotopic constraints from the millennium eruption. *Gondwana Research*, 68:13–21, 2019.

A. Derkachev, I. Utkin, N. Nikolaeva, S. Gorbarenko, G. Malakhova, M. V. Portnyagin, V. Sakhno, X. Shi, and H. Lv. Tephra layers of large explosive eruptions of baitoushan/changbaishan volcano in the japan sea sediments. *Quaternary International*, 2019.

T. Furuta, K. Fujioka, and F. Arai. Widespread submarine tephras around japan—petrographic and chemical properties. *Marine Geology*, 72(1-2):125–142, 1986.

W. Haiquan, L. Ruoxin, F. Qicheng, Y. Qingfu, and L. Ni. The tianchi volcano in the changbai mountains, northeast china——apolygenetic central volcano. *Geological Review*, 45:257–262, 1999.

Y. Hayakawa and M. Koyama. Dates of two major eruptions from towada and baitoushan in the 10th century. *Bulletin of the Volcanological Society of Japan*, 43(5):403–407, 1998.

R. Holasek, S. Self, and A. Woods. Satellite observations and interpretation of the 1991 mount pinatubo eruption plumes. *Journal of Geophysical Research: Solid Earth*, 101(B12):27635–27655, 1996.

S. Horn and H.-U. Schmincke. Volatile emission during the eruption of baitoushan volcano (china/north korea) ca. 969 ad. *Bulletin of Volcanology*, 61(8):537–555, 2000.

P. D. Hughes, G. Mallon, A. Brown, H. Essex, J. Stanford, and S. Hotes. The impact of high tephra loading on late-holocene carbon accumulation and vegetation succession in peatland communities. *Quaternary Science Reviews*, 67:160–175, 2013.

J. Kandlbauer and R. Sparks. New estimates of the 1815 tambora eruption volume. *Journal of Volcanology and Geothermal Research*, 286:93–100, 2014.

T. Koyaguchi and M. Tokuno. Origin of the giant eruption cloud of pinatubo, june 15, 1991. *Journal of Volcanology and Geothermal Research*, 55(1-2):85–96, 1993.

T. Kuritani, M. Nakagawa, J. Nishimoto, T. Yokoyama, and T. Miyamoto. Magma plumbing system for the millennium eruption at changbaishan volcano, china: Constraints from whole-rock uth disequilibrium. *Lithos*, page 105564, 2020.

Q. Liu, J. Liu, X. Chen, H. You, G. Chu, J. Han, J. Mingram, G. Schettler, and J. Negendank. Stable carbon isotope record of bulk organic matter from the sihailongwan maar lake, northeast china during the past 18.5 ka. *Quaternary Sciences*, 25(6):711–721, 2005.

R. Liu, H. Wei, J. Li, et al. Recent eruptions of the changbaishan tianchi volcano. *Sci. Press, Beijing*, page 165, 1998.

H. Machida and F. Arai. Extensive ash falls in and around the sea of japan from large late quaternary eruptions. *Journal of Volcanology and Geothermal Research*, 18(1-4):151–164, 1983.

H. Machida, H. Moriwaki, and D.-C. Zhao. The recent major eruption of changbai volcano and its environmental effects. *Geographical Reports of Tokyo Metropolitan University*, (25):1–20, 1990.

D. McLean, P. G. Albert, T. Nakagawa, R. A. Staff, T. Suzuki, V. C. Smith, et al. Identification of the changbaishan 'millennium'(b-tm) eruption deposit in the lake suigetsu (sg06) sedimentary archive, japan: synchronisation of hemispheric-wide palaeoclimate archives. *Quaternary Science Reviews*, 150:301–307, 2016.

D. McLean, P. G. Albert, T. Suzuki, T. Nakagawa, J.-I. Kimura, Q. Chang, A. Macleod, S. Blockley, R. A. Staff, K. Yamada, et al. Refining the eruptive history of ulleungdo and changbaishan volcanoes (east asia) over the last 86 kyrs using distal sedimentary records. *Journal of Volcanology and Geothermal Research*, 389:106669, 2020.

R. Nakanishi, J. Ashi, and S. Okamura. A dataset for distribution and characteristics of holocene pyroclastic fall deposits along the pacific coasts in western hokkaido, japan. *Data in Brief*, 33:106565, 2020.

F. Nanayama, K. Satake, R. Furukawa, K. Shimokawa, B. F. Atwater, K. Shigeno, and S. Yamaki. Unusually large earthquakes inferred from tsunami deposits along the kuril trench. *Nature*, 424(6949):660–663, 2003.

M. Okuno, M. Torii, K. Yamada, Y. Shinozuka, T. Danhara, K. Gotanda, H. Yonenobu, and Y. Yasuda. Widespread tephras in sediments from lake ichi-no-megata in northern japan: Their description, correlation and significance. *Quaternary International*, 246(1-2):270–277, 2011.

C. Oppenheimer, L. Wacker, J. Xu, J. D. Galván, M. Stoffel, S. Guillet, C. Corona, M. Sigl, N. Di Cosmo, I. Hajdas, et al. Multi-proxy dating the 'millennium eruption'of changbaishan to late 946 ce. *Quaternary Science Reviews*, 158:164–171, 2017.

B. Pan, S. L. de Silva, J. Xu, Z. Chen, D. P. Miggins, and H. Wei. The vei-7 millennium eruption, changbaishan-tianchi volcano, china/dprk: New field, petrological, and chemical constraints on stratigraphy, volcanology, and magma dynamics. *Journal of Volcanology and Geothermal Research*, 343:45–59, 2017.

B. Pan, S. L. de Silva, J. Xu, S. Liu, and D. Xu. Late pleistocene to present day eruptive history of the changbaishan-tianchi volcano, china/dprk: New field, geochronological and chemical constraints. *Journal of Volcanology and Geothermal Research*, page 106870, 2020.

F. C. Ramos, M. Heizler, J. Buettner, J. Gill, H. Wei, C. Dimond, and S. Scott. U-series and 40ar/39ar ages of holocene volcanic rocks at changbaishan volcano, china. *Geology*, 44(7):511–514, 2016.

F. C. Ramos, J. Wolff, J. Buettner, H. Wei, and J. Xu. Ra/th ages of sanidine in young trachytes erupted at changbaishan volcano, china. *Journal of Volcanology and Geothermal Research*, 374:226–241, 2019.

N. Razjigaeva, L. Ganzey, T. Grebennikova, L. Mokhova, K. A. Arslanov, F. Maksimov, A. Y. Petrov, and V. Sakhno. B–tm ash of a catastrophic eruption of baitoushan volcano in terrestrial deposits of primorye as an age marker of the medieval warm period in the holocene. In *Doklady Earth Sciences*, volume 494, pages 779–786. Springer, 2020.

L. Shi, X. Chen, W. H. Yang, Qingfu, and C. Lin. Petrochemistry of pumices of various colors produced by the eruption of changbaishan tianchi volcano at 1000 years ago. *Seismology and Geology*, 27(1):73–82, 2005.

C. Sun, G. Plunkett, J. Liu, H. Zhao, M. Sigl, J. R. McConnell, J. R. Pilcher, B. Vinther, J. Steffensen, and V. Hall. Ash from changbaishan millennium eruption recorded in greenland ice: implications for determining the eruption's timing and impact. *Geophysical Research Letters*, 41(2):694–701, 2014a.

C. Sun, H. You, J. Liu, X. Li, J. Gao, and S. Chen. Distribution, geochemistry and age of the millennium eruptives of changbaishan volcano, northeast china—a review. *Frontiers of Earth Science*, pages 1–15, 2014b.

C. Sun, H. You, H. He, L. Zhang, J. Gao, W. Guo, S. Chen, Q. Mao, Q. Liu, G. Chu, et al. New evidence for the presence of changbaishan millennium eruption ash in the longgang volcanic field, northeast china. *Gondwana Research*, 28(1):52–60, 2015.

C. Sun, J. Liu, H. You, and G. Chu. Clinopyroxene and fe-ti oxides for correlating the ash from changbaishan millennium eruption. *Science China Earth Sciences*, 59(7):1454–1462, 2016.

C. Sun, J. Liu, H. You, and K. Nemeth. Tephrostratigraphy of changbaishan volcano, northeast china, since the mid-holocene. *Quaternary Science Reviews*, 177:104–119, 2017.

H. Wei, R. Sparks, R. Liu, Q. Fan, Y. Wang, H. Hong, H. Zhang, H. Chen, C. Jiang, J. Dong, et al. Three active volcanoes in china and their hazards. *Journal of Asian Earth Sciences*, 21(5):515–526, 2003.

H. Wei, Y. Wang, J. Jin, L. Gao, S.-H. Yun, and B. Jin. Timescale and evolution of the intracontinental tianchi volcanic shield and ignimbrite-forming eruption, changbaishan, northeast china. *Lithos*, 96(1-2): 315–324, 2007.

H. Wei, G. Liu, and J. Gill. Review of eruptive activity at tianchi volcano, changbaishan, northeast china: implications for possible future eruptions. *Bulletin of volcanology*, 75(4):706, 2013.

H. Wei, B. Zhao, Z. Chen, and H. Yu. Volcanic processes and magmatic evolution of tianchi volcano, changbaishan. *Geological Society, London, Special Publications*, 510(1):15–26, 2021.

J. Xu, B. Pan, T. Liu, I. Hajdas, B. Zhao, H. Yu, R. Liu, and P. Zhao. Climatic impact of the millennium eruption of changbaishan volcano in china: New insights from high-precision radiocarbon wiggle-match dating. *Geophysical Research Letters*, 40(1):54–59, 2013.

Q. Yang, S. F. Jenkins, G. A. Lerner, W. Li, T. Suzuki, D. McLean, A. Derkachev, I. Utkin, H. Wei, J. Xu, et al. The millennium eruption of changbaishan tianchi volcano is vei 6, not 7. *Bulletin of Volcanology*, 83(11):1–10, 2021.

J. Yin, A. T. Jull, G. S. Burr, and Y. Zheng. A wiggle-match age for the millennium eruption of tianchi volcano at changbaishan, northeastern china. *Quaternary Science Reviews*, 47:150–159, 2012.

668 H. Yu, J. Xu, P. Luan, B. Zhao, and B. Pan. Probabilistic assessment of tephra fallout hazard at changbaishan
669 volcano, northeast china. *Natural hazards*, 69(3):1369–1388, 2013.

670 M. Zhang, Z. Guo, J. Liu, G. Liu, L. Zhang, M. Lei, W. Zhao, L. Ma, V. Sepe, and G. Ventura. The
671 intraplate changbaishan volcanic field (china/north korea): A review on eruptive history, magma genesis,
672 geodynamic significance, recent dynamics and potential hazards. *Earth-science reviews*, 187:19–52, 2018.

673 M. Zhang, Z. Bu, X. Wang, P. He, J. Chen, and Y. Cui. Petrochemical characteristics and geological
674 significance of the tephra buried under peat deposits: Constrains on the changbaishan millennium eruption.
675 *Catena*, 209:105857, 2022a.

676 M. Zhang, J. P. Smol, and Z. Bu. Late holocene tephrostratigraphic sequence of the changbaishan volcanic
677 field, china/north korea. *Gondwana Research*, 2022b.

678 B. Zhao, J. Xu, H. Yu, and Z. Chen. Pyroclastic density current facies in the millennium eruption of
679 tianchi volcano, northeast china: Insights from topography, stratigraphy, granulometry, and petrogra-
680 phy. *Frontiers in Earth Science*, 8:323, 2020. ISSN 2296-6463. doi: 10.3389/feart.2020.00323. URL
681 https://www.frontiersin.org/article/10.3389/feart.2020.00323.

682 H. Zou, Q. Fan, and H. Zhang. Rapid development of the great millennium eruption of changbaishan (tianchi)
683 volcano, china/north korea: evidence from u–th zircon dating. *Lithos*, 119(3-4):289–296, 2010.